Original Article

Prediction of start and finish transformation temperatures for different types of weld metals via machine learning

Tadeu Messias Donizete Borba [1]*
Louriel Oliveira Vilarinho [2]

Abstract

The interactions of different alloying elements in metallic alloys, combined with the application of thermal cycles and/or welding operations, have a significant impact on the microstructural characteristics and mechanical properties of materials. Continuous cooling transformation (CCT) diagrams, typically obtained through dilatometric tests, describe phase transformations in specific alloys during thermal cycling. However, this methodology requires long processing times, specialized equipment, and expertise, making it unsuitable for fast decision-making. This work presents a Machine Learning-based model, developed and validated to predict austenite decomposition during continuous cooling, using a dataset of experimental CCT diagrams of different weld metals available in the literature. The results demonstrate that the CCT diagrams predicted by the Machine Learning approach can be used as a promising tool to assist in studying microstructural changes occurring during the continuous cooling of weld metals. Moreover, this method can complement dilatometric analysis, reducing experimental time and costs while providing fast and accurate responses that could support the development of welding procedures.

Keywords: CCT Diagrams; Weld metal; Machine learning.

1 Introduction

The influence of fusion joining processes, particularly electric arc welding, on microstructural variations has been extensively evaluated in research studies, as it is one of the main factors affecting the mechanical properties of welded components. The extent and intensity of microstructural changes depend on, among other factors, the chemical composition of the materials and, most importantly, on the thermal cycles generated during the welding process [1-5]. Dilatometry is one of the techniques used to assess the effects of different thermal cycles on microstructural transformations by analyzing dimensional changes in test specimens. This method enables the determination of critical transformation temperatures, among other characteristics, allowing the construction of continuous cooling transformation (CCT) diagrams for different kinds of materials [6-10]. With a CCT diagram, it is possible to predict the effect of a given cooling rate on the transformation start and finish temperatures and/or the fraction of a specific microconstituent formed.

Although numerous CCT diagrams are available in the literature, few are directly applicable to welding studies due to two main limitations: (i) the slow heating rates typically used, generally below 5 ºC/s, and (ii) the use of low austenitization temperatures, which result in smaller austenitic grain sizes than those usually observed in welded regions, particularly in the weld metal and the coarse-grained region of the heat-affected zone [1-5,11]. Moreover, the application of this technique remains highly restricted due to the need for specialized equipment, such as the Gleeble and dilatometers, as well as expert knowledge and a relatively long testing time. As a result, it may not be the most suitable tool for rapid decision-making in material development and application.

For weld metals specifically, predicting the temperatures at which austenite starts and finishes transforming during continuous cooling is even more critical than understanding the transformations of individual microconstituents. Issues such as the susceptibility to hydrogen-induced cold cracking, the occurrence of solidification cracks, the formation of residual stress fields, and the development of brittle microstructures are all directly related to variations in the temperature range at which austenite decomposition occurs during the cooling of the welded joint [1-5,12,13].

Therefore, to assist in determining the optimal welding conditions, it is essential to have prior knowledge of the CCT diagrams of weld metals used in the production of critical components with stringent requirements, such as offshore structures, pressure vessels, military vehicles, and aerospace and nuclear equipment [14-16]. The transformation curves of CCT diagrams depend on the chemical composition of the

[1]*Centro de Pesquisa e Desenvolvimento, Usiminas, Ipatinga, MG, Brasil.*
[2]*Departamento de Engenharia Mecânica, Universidade Federal de Uberlândia – UFU, Uberlândia, MG, Brasil.*

**Corresponding author: tadeu.borba@usiminas.com*

metal alloy and the austenitic grain size subjected to cooling, which, in turn, is influenced by the austenitization temperature and holding time. Currently, as previously mentioned, CCT diagrams can be determined through physical simulation. However, this approach requires significant investment and time.

An alternative methodology involves using empirical equations or mathematical models to calculate transformation temperatures, enabling the construction of CCT diagrams [17-20]. These models consider grain size, austenitization temperature, effective diffusion coefficients, cooling rate, and specific coefficients for each chemical element in the alloy. Such equations serve as the foundation for software dedicated to studying microstructural transformations [21]. However, theoretical and mathematical models cannot precisely calculate transformation temperatures due to their inherent non-linearity [22].

As a result, a third method that has gained significant recognition in recent years for evaluating phase transformations in metal alloys and thus determining CCT diagrams is the application of machine learning techniques, artificial neural networks (ANNs), and statistical models. Machine learning models excel at identifying correlations among multiple variables under non-linear conditions, enabling highly accurate predictions. Owing to their low dependence on expensive software or high-performance computing systems and primarily due to their ease of implementation machine learning techniques have been widely applied to solve various industrial challenges, support materials design, and assist in the development of new alloys [23-27].

These approaches enable the prediction, modeling, and analysis of non-linear transformation curves based on a database of experimental CCT diagrams, allowing the evaluation of the influence of alloying elements and their interactions on the transformation kinetics [28–38]. In this study, models were developed and validated for predicting the start and finish temperatures of austenite transformation during the cooling of different types of weld metals. To achieve this, various machine learning model (MML) strategies were assessed, and the most suitable algorithms for this application were determined through a comparative analysis of correlation coefficients and mean absolute error (MAE) and root mean squared error (RMSE) values.

2 Methodology

2.1 Database construction

Figure 1 presents a flowchart illustrating the entire database construction process. The database for this study was developed based on 68 CCT diagrams of different weld metal types, 56 of which were extracted from the work of Zhang and Farrar [39], who compiled various results from the literature into an atlas. Additionally, 12 more CCT diagrams were obtained from the studies of Ito et al. [40,41].

Figure 2 provides examples of the diagrams used in this work. As shown in this figure, the diagrams are graphical representations of transformation temperature variation curves as a function of cooling time. To construct the database for model development, each CCT diagram was digitized and processed using the free software WebPlotDigitizer [42].

This tool enabled the extraction of transformation temperatures (T°T) and cooling times (tR). Through this procedure, 2813 data pairs were obtained for the start of austenite transformation and 2690 data pairs for the finish of austenite transformation. Additionally, the chemical composition data associated with each diagram were collected. Table 1 presents examples of the chemical compositions of some selected alloys, along with the range of each element's content, based on the entire evaluated database. Notably, the modeling was carried out considering the collective range of each element, without clustering, due to limited data availability for some alloys. Thus, the input parameters for the models included chemical composition, austenitization temperature (AT), and cooling rate (Rate), which was calculated based on the tR for a given T°T and AT, following Equation 1 [38]. The transformation temperatures at different cooling rates served as the output data for the models.

$$Rate = \left(AT - T°T\right) / tR \tag{1}$$

2.2 Modeling with different machine learning algorithms

Figure 3 presents a flowchart illustrating the steps used to predict CCT diagrams using the machine learning model.

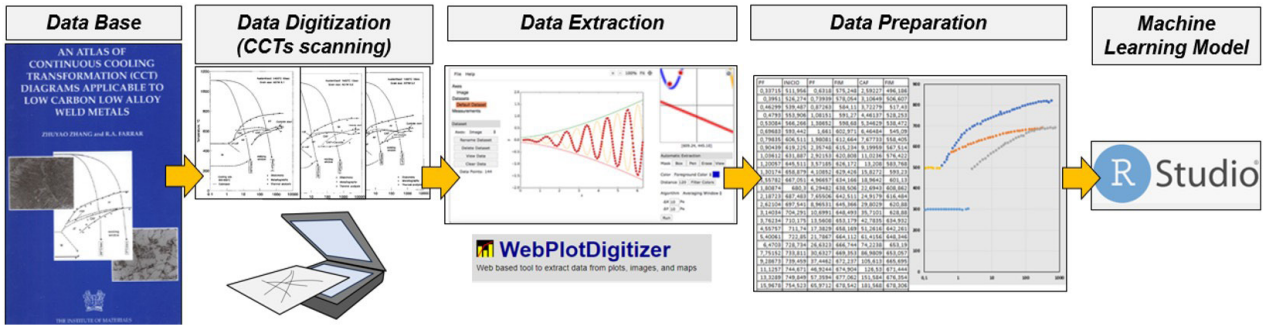

Figure 1. Diagram illustrating the main steps for creating the MML.

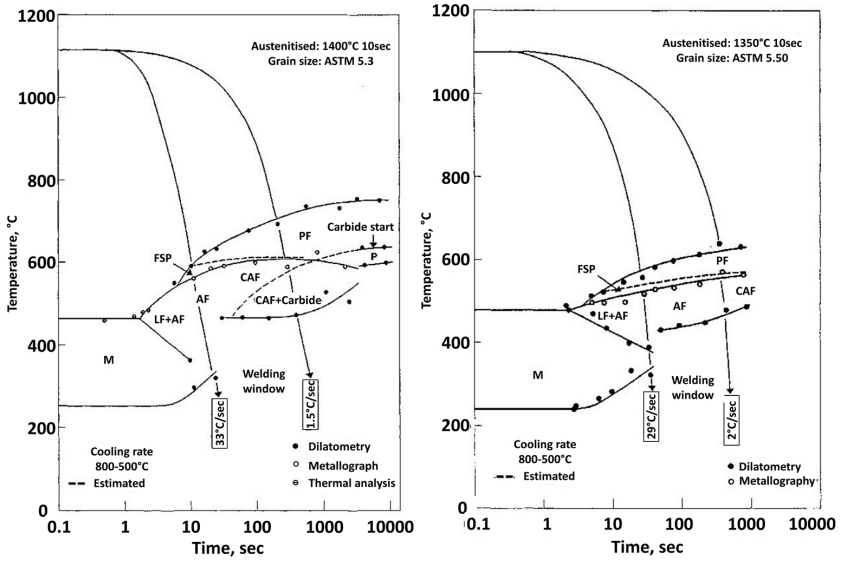

(a) CMnNi [32] (b) CMnNb [32]

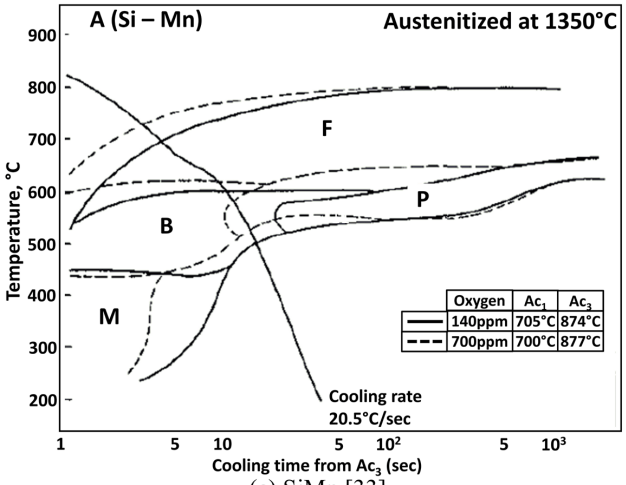

(c) SiMn [33]

Figure 2. Example of diagrams used in this work.

Table 1. Example of the chemical composition of some alloys used in this work and the range of each element (wt.%)

	C	Mn	Si	S	P	Cu	N	O	Ni	Cr	Mo	Ti	Al	B	Nb	V	CE	Pcm
CMn	0.06	0.56	0.41	0.008	0.023	0.04	0.007	0.041	0.05	---	---	---	---	---	---	---	0.18	0.10
CMnNi	0.04	1.20	0.41	0.014	0.024	0.05	0.012	0.043	1.10	0.01	0.07	---	---	---	0.01	---	0.35	0.16
CMnNiMo	0.06	1.50	0.37	0.009	0.015	0.06	0.005	0.020	0.96	0.01	0.23	0.018	0.003	---	---	---	0.43	0.18
CMnSi	0.11	0.74	0.09	0.013	0.016	0.12	0.005	0.071	0.03	0.00	---	---	---	---	---	---	0.25	0.16
Minimum	0.02	0.56	0.09	0.005	0.002	---	---	---	---	---	---	---	---	---	---	---	0.16	0.09
Maximum	0.12	2.10	0.67	0.025	0.030	0.46	0.031	0.114	5.53	0.35	0.45	0.050	0.060	0.0045	0.03	0.11	0.59	0.22

CE = C + Mn/6 + (Ni + Cu)/15 + (Cr + Mo + V)/5; Pcm = C + Si/30 + (Mn + Cu + Cr)/20 + Ni/60 + Mo/15 + V/10 + 5B.

During the training phase of this study, different algorithms were tested to determine those best suited for predicting CCT diagrams. The following models were evaluated: General Linear Regression (GLM), Elastic Net Regression (GLMNET), k-Nearest Neighbors (KNN), Random Forest (RF), Support Vector Machine (SVM), Decision Trees-Rule-Based Cubist (CUBIST), and Extreme Gradient Boosting (XGB) [43-45]. Among these, KNN stands out as a simple yet widely applied algorithm for various regression problems. In KNN regression, the predicted output is the average value of the k nearest neighbors [43-45].

As an ensemble decision tree algorithm, RF builds multiple statistical approximations to develop a predictive model. It offers superior computational accuracy compared to most individual algorithms and, due to its inherent randomness, demonstrates strong generalization capabilities and resistance

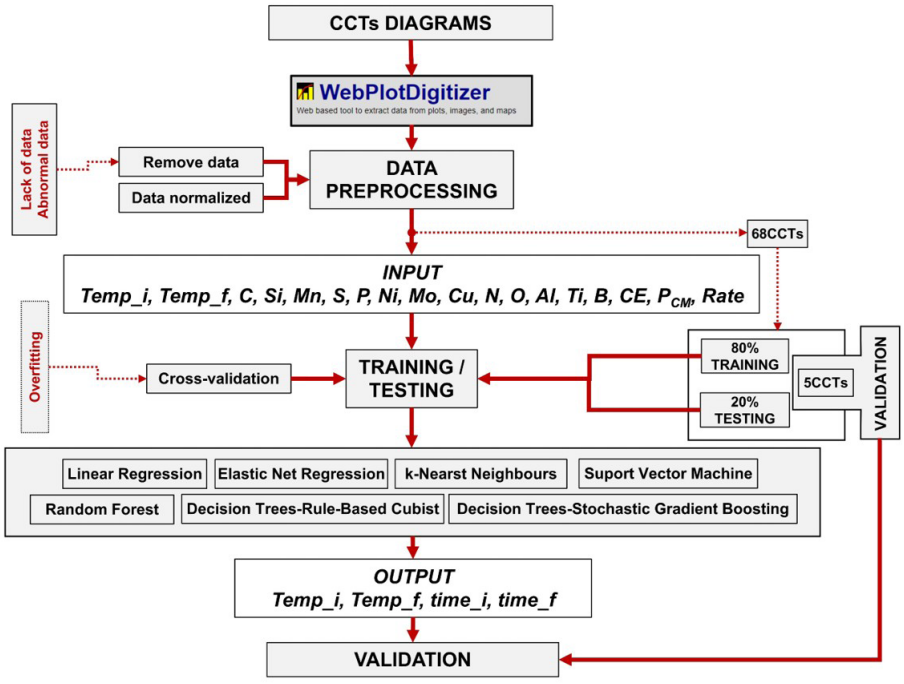

Figure 3. Steps Used To Predict CCT Diagrams Via Machine Learning.

to overfitting. This makes it particularly suitable for handling complex nonlinear multivariate problems without requiring explicit feature selection [43-45].

Overfitting during training is often as significant as the performance differences between learning algorithms and, therefore, cannot be ignored in an empirical evaluation. To mitigate overfitting in nonlinear regression problems and maximize data usage, k-fold cross-validation was applied. In this method, the original dataset is randomly divided into k equal-sized subsamples. Of these, one subsample is retained for model validation, while the remaining (k – 1) subsamples are used for training. This process is repeated k times, ensuring that each subsample is used exactly once for validation. The final performance metric is obtained by averaging the results from all k iterations. A key advantage of this approach is that all observations are utilized for both training and validation, enhancing model robustness.

The literature suggests that stratified cross-validation with 10 to 20 folds is optimal for model selection, even when computational resources allow for more subsets [46]. Consequently, in this study, k = 20 was used.

Following this, the different models were trained to predict the start and finish temperatures of austenite transformation. To quantitatively assess the regression performance, the R^2 (coefficient of determination) and error metrics were computed. It's a well-known fact that the R^2 value ranges from 0 to 1, with values closer to 1 indicating better correlation. Generally, a model is considered highly correlated when $R^2 > 0.8$ [45]. Additionally, the mean absolute error and root mean squared error were used to evaluate and compare prediction quality among the models [43-45].

Thus, the lower the MAE and RMSE values and the higher the R^2 value, the more consistent and accurate the predicted transformation temperatures will be across different cooling rates.

After preprocessing, each dataset corresponded to a CCT diagram with 15 numerical attributes (features). The qualitative relationship between the transformation start (Temp_i) and finish (Temp_f) temperatures and the selected features can be described by Expressions 2 and 3. To evaluate the machine learning procedure, data from five CCT diagrams, which were not included in the training phase, were set aside for validation, while the remaining dataset was split into 80% for training and 20% for testing. Additionally, all data were centered and normalized before training.

$$Temp\_i = F\left(C, Mn, Si, O, N, S, P, Cu, Mo, Ni, Al, Ti, CE, P_{cm}, Rate\right) \quad (2)$$

$$Temp\_f = F\left(C, Mn, Si, O, N, S, P, Cu, Mo, Ni, Al, Ti, CE, P_{cm}, Rate\right) \quad (3)$$

3 Results and discussion

3.1 Data evaluation

Although austenitic grain size, austenitization time, and heating rate are essential variables for determining transformation temperatures, these parameters were not considered in this evaluation due to the lack of information in several diagrams, as shown in Figure 4.

Prior to training the models, a comprehensive assessment of the entire database was conducted. Data

deemed incorrect or anomalous were removed from the training dataset based on prior knowledge of dilatometric tests and principles of physical and welding metallurgy. However, while this database adjustment was necessary, the exclusion of these variables may represent a limitation of the models presented in this study.

To verify the consistency of the data, Pearson correlation graphs were generated, as shown in Figure 5a, to assess the collinearity among the variables.

In general, as expected, most alloying elements inversely affect the Temp_i and Temp_f, lowering them as their content increases. This behavior is attributed to the increased hardenability of the alloys.

The cooling rate (Rate) also exhibits an inverse correlation with Temp_i and Temp_f, which is consistent with the well-established understanding that more severe cooling promotes the formation of low-temperature transformation constituents [47-49]. An intriguing result is the strong effect of oxygen, which appears to increase Temp_i and Temp_f. This phenomenon is believed to be associated with heterogeneous nucleation occurring during weld metal solidification due to the presence of globular

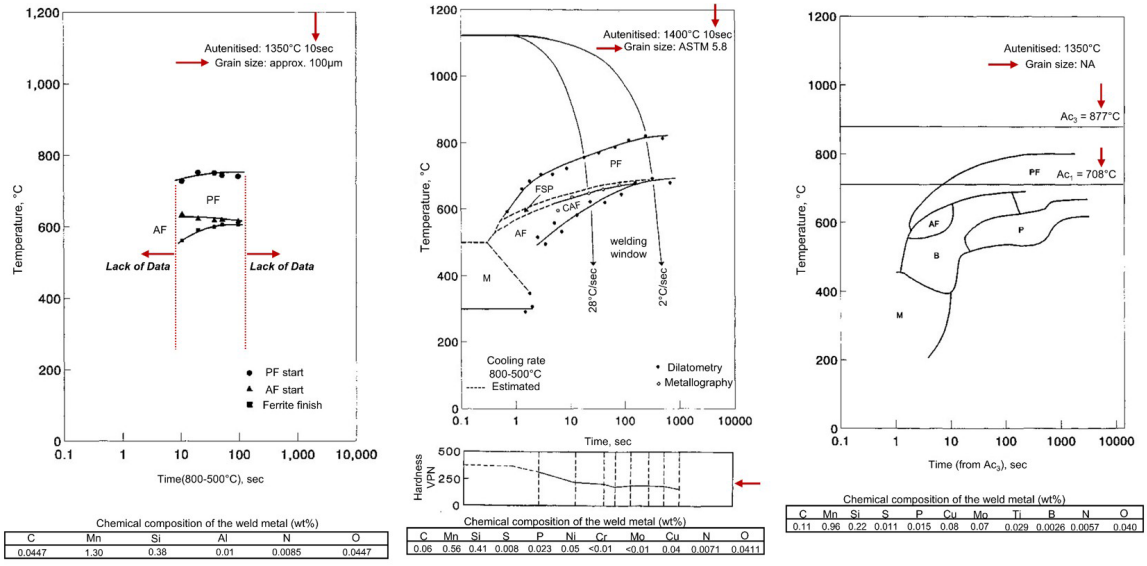

Figure 4. Some examples of the diagrams used in the construction of the database. The red arrows indicate the differences found in the diagrams [39].

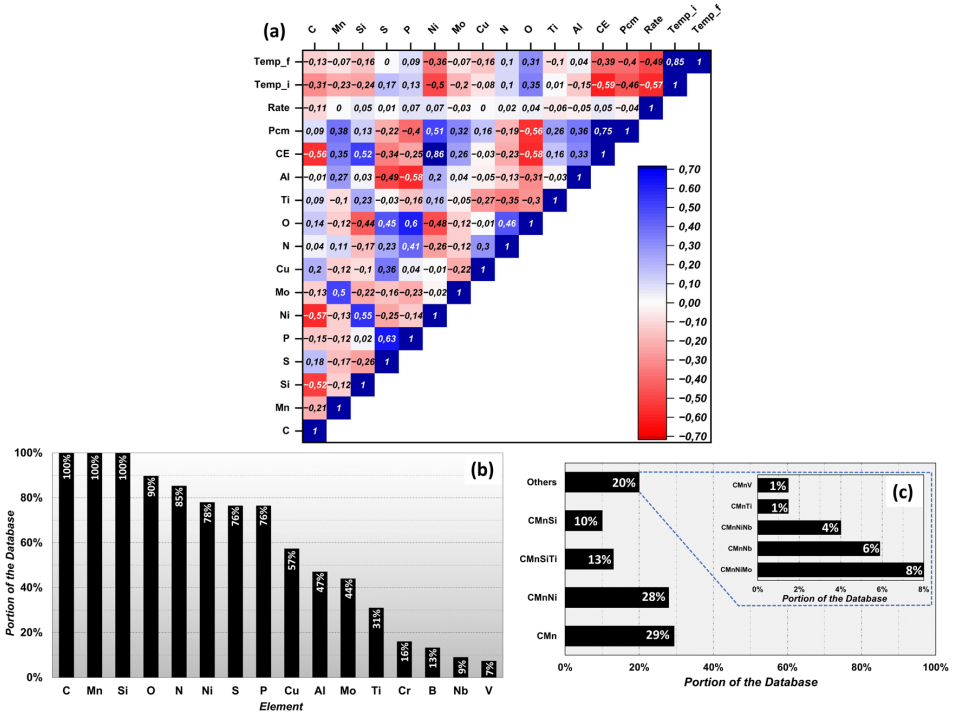

Figure 5. Pearson correlation map (a), participation of alloy elements (b) and distribution of alloy types (c) in the database used.

oxides. This strategy is commonly used to promote acicular microstructures and grain refinement, thereby facilitating austenitic transformation at higher temperatures [1-5,40,41].

Figure 5b illustrates the distribution of alloying elements in the database. As expected, the alloys are primarily composed of C, Mn, and Si, given that these elements are fundamental in welding carbon and low-alloy steels. Another notable observation is that reductions in carbon content tend to be compensated by increased additions of Mn, Si, Ni, and Mo, a strategy commonly employed to balance the effects of carbon in the design of high-strength steel alloys [47-49]. However, other alloying elements, such as V, Nb, Cr, and B, are less represented in the dataset. For this reason, they were excluded from the training stage due to their limited presence, particularly the element B, which significantly affects the transformation temperatures [47-49].

This limited presence of certain elements can be attributed to multiple factors: (i) some alloy designs may not include specific elements in their composition, and/or (ii) certain elements may have been omitted or undetected due to the analytical techniques used, meaning their absence in the database does not necessarily imply that they are absent in the actual weld metals. Another important aspect is the type of alloy studied.

As shown in Figure 5c, nearly half of the dataset consists of C-Mn-Ni alloys, indicating that the model developed in this study is best suited for predicting transformation behaviors in these types of alloys. A limited dataset for specific elements can significantly impact the performance of a machine learning model, potentially leading to: (i) Overfitting in dominant variables, (ii) Underfitting for variables with low representation, (iii) Less reliable predictions, and (iv) Imbalance and bias in the model. Since additional CCT diagrams for weld metals could not be obtained from the literature to enrich the dataset with underrepresented elements, alternative strategies were implemented. In addition to overfitting control and regularization techniques, robust models capable of handling imbalanced data such as decision trees, random forests, and gradient boosting were evaluated to enhance prediction reliability.

3.2 Prediction of start and finish transformation temperatures

Figure 6 presents a comparison of the MAE and RMSE error values obtained for each trained model, considering cross-validation. It can be observed that the RF (Random Forest), CUBIST, and XGB (Extreme Gradient Boosting) models achieved the lowest MAE and RMSE values in the training sets for predicting the Temp_i and Temp_f of austenite transformation.

Among these, the RF algorithm demonstrated the best performance for Temp_i, with a variation of ± 18 °C, while XGB was the most accurate for Temp_f, with a variation of ± 34 °C. These deviations are considered acceptable and are commonly observed in dilatometric experimental practice.

Figure 7 presents a comparison of the R^2 values obtained for each trained model. As with the error metrics, the models that achieved the highest R^2 values for predicting

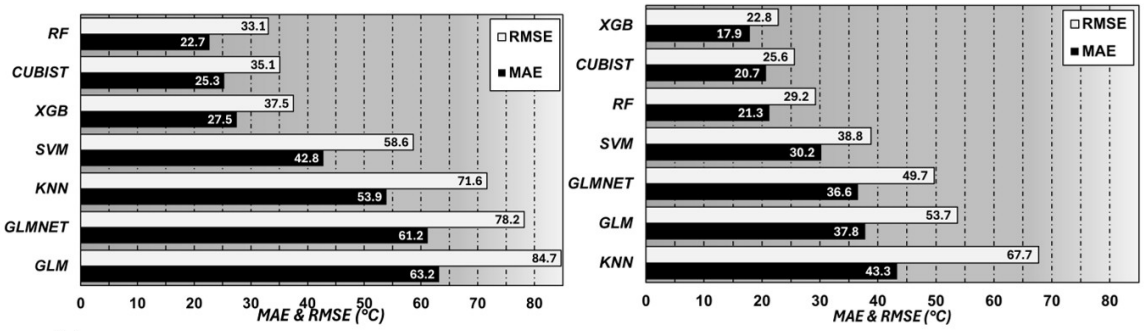

(a) Start Transformation Temperature (b) Finish Transformation Temperature

Figure 6. Comparison of algorithms through error values on the training set.

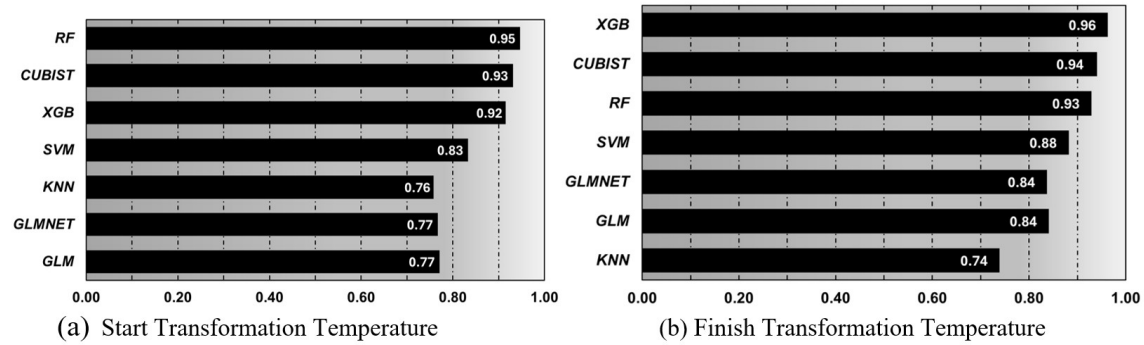

(a) Start Transformation Temperature (b) Finish Transformation Temperature

Figure 7. Comparison of algorithms through R^2 values on the training set.

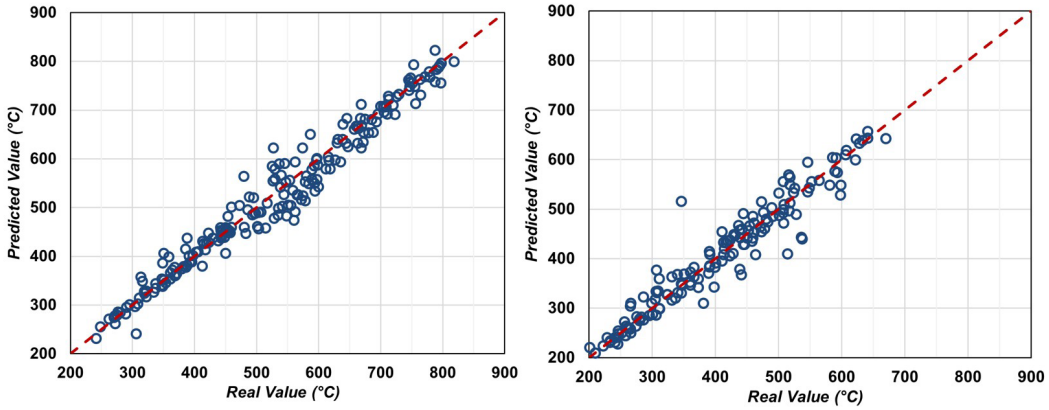

(a) Start Transformation Temperature (b) Finish Transformation Temperature

Figure 8. Performance of the machine learning models on the training set.

the start (Temp_i) and finish (Temp_f) temperatures were RF, CUBIST, and XGB. Among them, XGB exhibited the best performance for Temp_i, with $R^2 = 0.95$, while RF achieved the highest accuracy for Temp_f, with $R^2 = 0.96$.

Figure 8 illustrates the performance of the best models by comparing predicted vs. actual values (or real values). Most data points are concentrated near the asymptotic line (45° oblique line), indicating a high prediction accuracy of the developed models.

As shown in Figure 9, where the effectiveness of the KNN model in predicting transformation temperatures was evaluated, it is evident that for intermediate times, the prediction accuracy deteriorates.

As will be demonstrated later, this issue is linked to the quality of the original dataset. Indeed, a preliminary evaluation of the models, shown in Figure 10, reveals that the dispersion of the difference between predicted and actual transformation temperatures (ΔT°T) is smaller when using XGB and RF compared to KNN and GLM, particularly for intermediate temperature ranges.

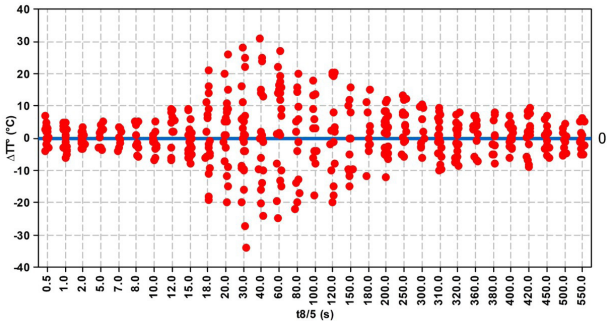

Figure 9. Dispersion of intermediate results in prediction efficiency via KNN.

3.3 Validation

To assess the predictive performance and effectiveness of the proposed methodology, the trained model was applied to predict the austenite transformation start (Temp_i) and finish (Temp_f) temperatures for three types of weld metals: one alloy containing only C-Mn, and two others with the addition of silicon (C-Mn-Si) and nickel (C-Mn-Ni). Figure 11 presents the experimental (real) data points overlapped on the CCT diagrams predicted by the machine learning model (MML). The results indicate that the trained MML achieved a good fit for all three weld metal types, with predicted transformation temperatures closely matching the experimental values.

This agreement is particularly strong for extreme conditions, i.e., at the lowest and highest cooling rates, and it is especially accurate for the transformation start temperature (Temp_i).

From a transformation kinetics perspective, occurrences at intermediate temperatures and times are the most challenging to determine experimentally and, consequently, the most difficult to predict. This is due to the nucleation and growth phenomena of microconstituents occurring in a mixed manner, involving both displacive and reconstructive mechanisms governed by atomic diffusion and crystal rearrangement, respectively [47-53].

Additionally, analyzing experimental dilatometric curves from which CCT diagrams are constructed is more complex for intermediate transformation temperatures. These evaluations are more susceptible to human interpretation, making them inherently prone to errors compared to the determination of low and high transformation temperatures. It is important to note that all experimental CCT diagrams available in the literature, including those used in this study, are constructed manually. In this process, a limited number of experimental data points are interpolated to form transformation temperature curves as a function of cooling time.

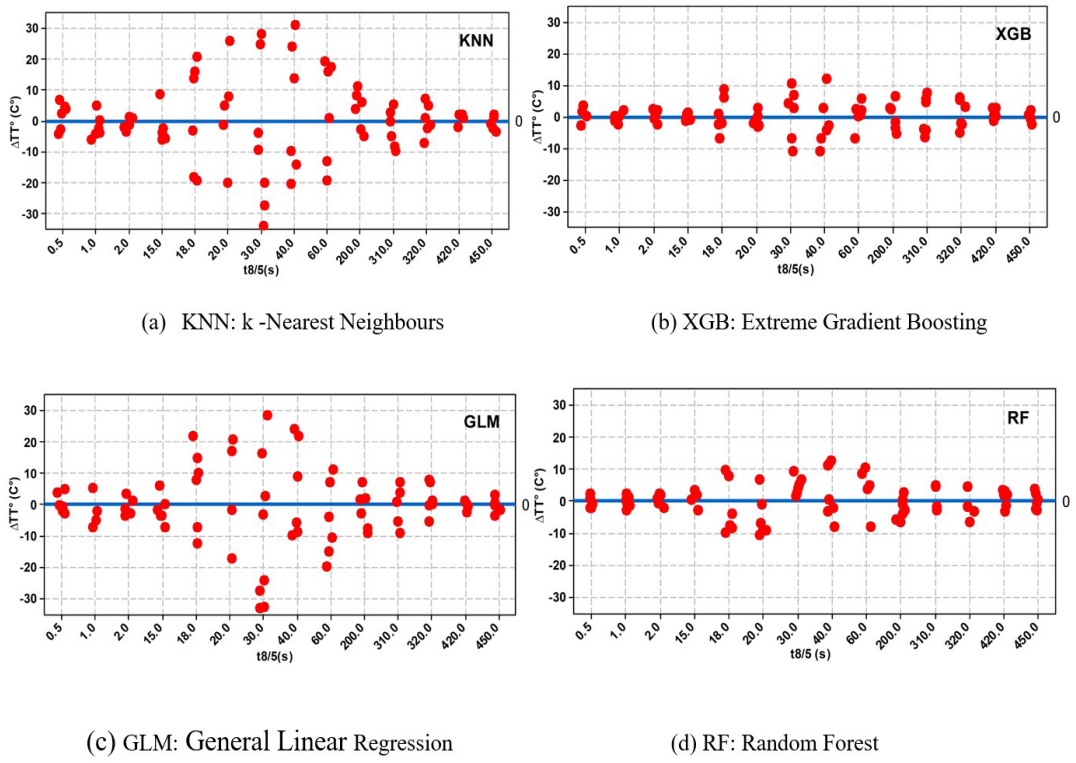

(a) KNN: k -Nearest Neighbours

(b) XGB: Extreme Gradient Boosting

(c) GLM: General Linear Regression

(d) RF: Random Forest

Figure 10. Comparison between KNN, GLM, XGB and RF models. ΔT°T = real temperature (original CCT) - predicted temperature.

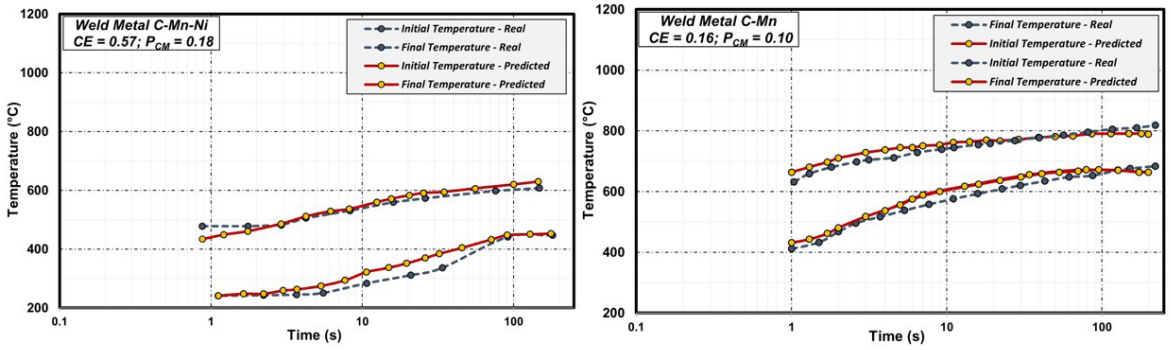

(a) CMnNi: CEQ = 0.57; P_{CM} = 0.18

(b) CMn. CEQ = 0.16; P_{CM} = 0.10

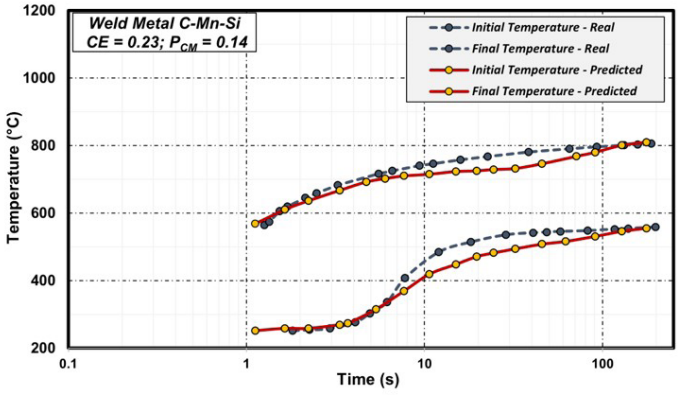

Figure 11. Comparison of the real data with the CCT diagram predicted by the developed machine learning model.

Furthermore, the model exhibited lower prediction errors for the C-Mn weld metal, followed by C-Mn-Ni and C-Mn-Si. This behavior may be attributed to differences in hardenability among the alloys, as well as the composition of the training database.

Compared to C-Mn alloys, the C-Mn-Ni and C-Mn-Si weld metals, due to their differences in chemical composition, are more sensitive to temperature variations, leading to the formation of different microconstituents in varying fractions at intermediate transformation temperatures [1-5,47-49]. This increased heterogeneity in microstructural transformations is difficult to detect in dilatometric tests, making transformation temperature detection highly dependent on human interpretation [47-53]. This introduces greater variability in experimental results, directly impacting the training process and predictive accuracy of the models.

In particular, for the C-Mn-Si alloy, it is believed that, in addition to the effects of chemical composition, the low representation of this material system (MS) in the training dataset (as shown in Figure 5c) may have negatively affected the accuracy of the developed machine learning model. This suggests that future studies should focus on expanding the training dataset to include more C-Mn-Si alloys. Thus, it is evident that MML training is inherently influenced by the subjectivity of the training data itself. An alternative approach to mitigate this issue in future research is to explore the clustering of transformation temperature groups and apply different models to predict transformation curves as a function of cooling rate variations. Additionally, increasing the availability of dilatometric test data could further improve model accuracy. However, the errors observed in the MML predictions can be considered acceptable deviations, as these variations in transformation temperatures are commonly encountered in dilatometric experimental practice.

4 Conclusion

This study presents an alternative approach to dilatometric thermophysical simulation for evaluating phase transformations in weld metals. In this context, different machine learning strategies were explored to predict CCT diagrams for various types of weld metals, using chemical composition data, austenitization temperature, and cooling rate as input parameters. For modeling, several algorithms were assessed, including General Linear Regression (GLM), Elastic Net Regression (GLMNET), k-Nearest Neighbors (KNN), Random Forest (RF), Support Vector Machine (SVM), Decision Trees-Rule-Based Cubist (CUBIST), and Extreme Gradient Boosting (XGB). The most suitable models were selected based on a comparative analysis of error metrics and R^2 values: (i) the RF model was chosen to predict the start austenite transformation temperatures during cooling e; (ii) the XGB model was selected to predict the final austenite transformation temperatures during cooling.

The models were validated, and the generated CCT diagrams exhibited acceptable deviations compared to experimental (real) results for C-Mn and C-Mn-Ni weld metals.

It is important to emphasize that the performance of the developed model is dependent on the training dataset and is constrained by the boundary conditions of the available data. Therefore, it is expected that the model will provide reasonably accurate predictions for weld metals whose chemical composition falls within the upper and lower limits of each element present in the training set.

Finally, the results of this study demonstrate that machine learning techniques provide a powerful computational approach for studying microstructural changes during the continuous cooling of weld metals. This methodology reduces the time and cost associated with dilatometric experiments, while also delivering fast and reliable predictions. Consequently, it serves as a valuable tool for developing optimized welding procedures for critical components with high safety and performance requirements, such as pressure vessels and military, aerospace, and nuclear applications.

Acknowledgements

The authors are grateful to the engineer Felipe Pereira Finamor for the support and knowledge transmitted in the creation of the MML. They are also grateful to Usiminas Research and Development Center for their support in carrying out the study.

References

1 Easterling KE, Easterling K. Introduction to the physical metallurgy of welding. Woburn: Butterworth-Heinemann; 2013.

2 Schulze G. Die Metallurgie des Schweißens - Eisenwerkstoffe und Nichteisenmetallische Werkstoffe. London: Springer; 2010. http://doi.org/10.1007/978-3-642-03183-0.

3 Granjon H. Fundamentals of welding metallurgy. Cambridge: Woodhead Publishing; 1991. http://doi.org/10.1533/9781845698805.

4 Linnert GE. Welding metallurgy: fundamentals. Vol. 1. 4th ed. Miami: American Welding Society; 1995.

5 Kou S. Welding metallurgy. 3rd ed. Nashville: John Wiley & Sons; 2020.

6 Vimalan G, Ravichandran G, Muthupandi V. Phase transformation behaviour in P91 during post weld heat treatment: a gleeble study. Transactions of the Indian Institute of Metals. 2017;70(3):875-885. http://doi.org/10.1007/s12666-017-1075-0.

7 Huang Q, Volkova O, Biermann H, Mola J. Dilatometry analysis of dissolution of Cr-rich carbides in martensitic stainless steels. Metallurgical and Materials Transactions. A, Physical Metallurgy and Materials Science. 2017;48(12):5771-5777. http://doi.org/10.1007/s11661-017-4377-2.

8 Shahriari B, Vafaei R, Sharifi EM, Farmanesh K. Continuous cooling transformation behavior and the kinetics of bainite formation in a bainitic–martensitic steel. International Journal of Materials Research. 2017;108(9):715-724.

9 López-Martínez E, Vázquez-Gómez O, Vergara-Hernández HJ, Campillo B. Effect of initial microstructure on austenite formation kinetics in high-strength experimental microalloyed steels. International Journal of Minerals Metallurgy and Materials. 2015;22(12):1304-1312. http://doi.org/10.1007/s12613-015-1198-4.

10 Caballero FG, Capdevila C, De Andrés CG. Modelling of kinetics and dilatometric behaviour of austenite formation in a low-carbon steel with a ferrite plus pearlite initial microstructure. Journal of Materials Science. 2002;37(16):3533-3540. http://doi.org/10.1023/A:1016579510723.

11 Borba TMD, Modenesi PJ. Influência do ciclo térmico de soldagem no crescimento de grão, nas transformações microestruturais e na formação de MA na GGZAC de aço TMCP. Soldagem e Inspeção. 2019;24:e2406. http://doi.org/10.1590/0104-9224/si24.06.

12 Bhatti AA, Barsoum Z, Murakawa H, Barsoum I. Influence of thermo-mechanical material properties of different steel grades on welding residual stresses and angular distortion. Materials & Design. 2015;65:878-889. http://doi.org/10.1016/j.matdes.2014.10.019.

13 Abreu SGPT, Porcaro RR, Faria GL, Godefroid LB, Pereira IC, Souza SS. Austenitizing temperature effects on the martensitic transformation and its influence on simulated welding residual stresses in a microalloyed-steel. Materials Research. 2023:26:e20220624.

14 Imai S. Recent progress and future trends for shipbuilding steel. Weld. Int. 2008;22(11):755-761. http://doi.org/10.1080/09507110802550661.

15 Kasuya T, Yurioka N, Okumura M. Methods for predicting maximum hardness of heat-affected zone and selecting necessary preheat temperature for steel welding. Nippon Steel Technical Report. 1995;65:7-14.

16 Yurioka N. Welding of TMCP steels. Journal of the Japan Welding Society. 1992;61(4):288-304. http://doi.org/10.2207/qjjws1943.61.4_288.

17 Pohjonen A, Somani M, Porter D. Modelling of austenite transformation along arbitrary cooling paths. Computational Materials Science. 2018;150:244-251. http://doi.org/10.1016/j.commatsci.2018.03.052.

18 Ollat M, Militzer M, Massardier V, Fabregue D, Buscarlet E, Keovilay F, et al. Mixed-mode model for ferrite-to-austenite phase transformation in dual-phase steel. Computational Materials Science. 2018;149:282-290. http://doi.org/10.1016/j.commatsci.2018.02.052.

19 Li MV, Niebuhr DV, Meekisho LL, Atteridge DG. A computational model for the prediction of steel hardenability. Metallurgical and Materials Transactions. B, Process Metallurgy and Materials Processing Science. 1998;29(3):661-672. http://doi.org/10.1007/s11663-998-0101-3.

20 Enomoto M. Prediction of TTT-diagram of proeutectoid ferrite reaction in iron alloys from diffusion growth theory. ISIJ International. 1992;32(3):297-305. http://doi.org/10.2355/isijinternational.32.297.

21 Saunders N, Guo Z, Miodownik AP, Schillé J-P. The calculation of TTT and CCT diagrams for general steels. JMatPro Software Literature, pp 1–12. http://www.thermotech.co.uk/resou rces/TTT_CCT_Steels.pdf. 2004.

22 Chakraborty S, Das P, Kaveti NK, Chattopadhyay PP, Datta S. MCDM towards knowledge incorporation in ANN models for phase transformation in continuous cooling of steel. Multidiscipline Modeling in Materials and Structures. 2019;15(1):170-186. http://doi.org/10.1108/MMMS-01-2018-0002.

23 Pan G, Wang F, Shang C, Wu H, Wu G, Gao J, et al. Advances in machine learning- and artificial intelligence-assisted material design of steels. International Journal of Minerals Metallurgy and Materials. 2023;30(6):1003-1024. http://doi.org/10.1007/s12613-022-2595-0.

24 Oliveira AP, Lourenço LS. Use of auto machine learning, artificial intelligence, for predictive modeling of metallurgical properties of hot-rolled steel products. Tecnologica em Metalurgia, Materiais e Mineração. 2025;22:e3149. http://doi.org/10.4322/2176-1523.20243149.

25 Duan H, He H, Yue S, Cao M, Zhao Y, Zhang Z, et al. Analysis of high-cycle fatigue life prediction of 304 stainless steel based on deep learning. Journal of the Minerals Metals & Materials Society. 2023;75(11):4586-4595. http://doi.org/10.1007/s11837-023-06042-8.

26 Srivastava AK, Patra PK, Jha R. AHSS applications in Industry 4.0: determination of optimum processing parameters during coiling process through unsupervised machine learning approach. Materials Today. Communications. 2022;31:103625. http://doi.org/10.1016/j.mtcomm.2022.103625.

27 Hamdi A, Merghache SM. Application of artificial neural networks (ANN) and gray relational analysis (GRA) to modeling and optimization of the material ratio curve parameters when turning hard steel. International Journal of Advanced Manufacturing Technology. 2023;124(10):3657-3670. http://doi.org/10.1007/s00170-023-10833-3.

28 Trzaska J, Jagiełło A, Dobrzanski LA. The calculation of CCT diagrams for engineering steels. Archives of Materials Science and Engineering. 2009;39(1):13-20.

29 Wang J, van der Wolk PJ, van der Zwaag S. Effects of carbon concentration and cooling rate on continuous cooling transformations predicted by artificial neural network. ISIJ International. 1999;39(10):1038-1046. http://doi.org/10.2355/isijinternational.39.1038.

30 Malinov S, Sha W, Guo Z. Application of artificial neural network for prediction of time–temperature–transformation diagrams in titanium alloys. Materials Science and Engineering: A. 2000;283(1-2):1-10.

31 Martin H, Amoako-Yirenkyi P, Pohjonen A, Frempong NK, Komi J, Somani M. Statistical modeling for prediction of CCT diagrams of steels involving interaction of alloying elements. Metallurgical and Materials Transactions. B, Process Metallurgy and Materials Processing Science. 2021;52(1):223-235. http://doi.org/10.1007/s11663-020-01991-w.

32 Pohjonen A, Somani M, Porter D. Effects of chemical composition and austenite deformation on the onset of ferrite formation for arbitrary cooling paths. Metals. 2018;8(7):540. http://doi.org/10.3390/met8070540.

33 Jiang X, Yin H-Q, Zhang C, Zhang R-J, Zhang K-Q, Deng Z-H, et al. An materials informatics approach to Ni-based single crystal superalloys lattice misfit prediction. Computational Materials Science. 2018;143:295-300. http://doi.org/10.1016/j.commatsci.2017.09.061.

34 García PJ No, García-Gonzalo E, Álvarez Antón JC, González Suárez VM, Mayo Bayón R, Mateos Martín F. A comparison of several machine learning techniques for the centerline segregation prediction in continuous cast steel slabs and evaluation of its performance. Journal of Computational and Applied Mathematics. 2018;330:877-895. http://doi.org/10.1016/j.cam.2017.02.031.

35 Trzaska J, Dobrzański LA. Modelling of CCT diagrams for engineering and constructional steels. Journal of Materials Processing Technology. 2007;192–193:504-510. http://doi.org/10.1016/j.jmatprotec.2007.04.099.

36 You W, Xu W, Liu Y, Bai B, Fang H. Effect of chromium on CCT diagrams of novel air-cooled bainite steels analyzed by neural network. Journal of Iron and Steel Research International. 2007;14(4):39-42. http://doi.org/10.1016/S1006-706X(07)60055-7.

37 Chakraborty S, Chattopadhyay PP, Ghosh SK, Datta S. Incorporation of prior knowledge in neural network model for continuous cooling of steel using genetic algorithm. Applied Soft Computing. 2017;58:297-306. http://doi.org/10.1016/j.asoc.2017.05.001.

38 Zhang B, Wang B, Xue W, Ullah A, Zhang T, Wang H. Development of a machine learning model for prediction of continuous cooling transformation diagrams in welding heat-affected zone. Journal of Materials Science. 2023;58(11):4795-4808. http://doi.org/10.1007/s10853-023-08322-9.

39 Zhang Z, Farrar RA. An atlas of continuous cooling transformation (CCT) diagrams applicable to low carbon low alloy weld metals. Bournemouth: The Institute of Materials; 1995.

40 Ito Y, Nakanishi M, Komizo Y. Effect of oxygen on transformation of low carbon weld metal. Study on microstructure and toughness of the weld metal (1st report). Journal of the Japan Welding Society. 1981;50(12):1211-1218. http://doi.org/10.2207/qjjws1943.50.1211.

41 Ito Y, Nakanishi M, Komizo Y. Hardenability of the weld metal compared with rolled steel plate. Study on microtructure and toughness of the weld metal (3rd report). Journal of the Japan Welding Society. 1982;51(4):354-359. http://doi.org/10.2207/qjjws1943.51.354.

42 Automeris LLC. Software WebPlotDigitizer [cited 2025 Mar 25]. Available at: https://automeris.io/WebPlotDigitizer/

43 W3Schools. Python Tutorial [cited 2025 Mar 25]. Available at: https://www.w3schools.com/python/default.asp

44 Scikit-learn. Sklearn [cited 2025 Mar 25]. Available at: https://scikit-learn.org/stable/modules/classes.html#module-sklearn.ensemble

45 Hastie T, Tibshirani R, Friedman J. The elements of statistical learning: data mining, inference, and prediction. 2nd ed. [cited 2025 Mar 25]. Available at: https://hastie.su.domains/ElemStatLearn/

46 Kohavi R. A study of cross-validation and bootstrap for accuracy estimation and model selection. IJCAI (United States). 1995;14(2):1137-1145.

47 Krauss G. Steels: processing, structure, and performance. 2nd ed. Materials Park: ASM International; 2015.

48 Bhadeshia H, Honeycombe R. Steels: microstructure and properties. 4th ed. Oxônia: Butterworth-Heinemann; 2017.

49 Bhadeshia HKD. Bainite in steels: theory and practice. 3rd ed. London: CRC Press; 2019.

50 Scotti A, Li H, Miranda RM. A round-robin test with thermal simulation of the welding HAZ to draw CCT diagrams: a need for harmonised procedures and microconstituent terminologies. Soldagem e Inspeção. 2014;19(3):279-290. http://doi.org/10.1590/0104-9224/SI1903.11.

51 Pawlowski B. Dilatometric examination of continuously heated austenite formation in hypoeutectoid steels. Journal of Achievements in Materials and Manufacturing Engineering. 2012;54(2):185-193.

52 Liu T, Long M, Fan H, Chen D, Chen H, Duan H, et al. Dilatometric determination of four critical temperatures and phase transition fraction for austenite decomposition in hypo-eutectoid steels using peak separation method. Journal of Materials Research. 2018;33(8):967-977. http://doi.org/10.1557/jmr.2017.484.

53 Leach L, Kolmskog P, Höglund L, Hillert M, Borgenstam A. Use of Fe-C information as reference for alloying effects on BS. Metallurgical and Materials Transactions. A, Physical Metallurgy and Materials Science. 2019;50(10):4531-4540. http://doi.org/10.1007/s11661-019-05371-1.

Received: 25 Mar. 2025
Accepted: 06 Jun. 2025

Editor-in-charge:
Paula Fernanda da Silva Farina